

Electromagnetic Tracking in High Dose Rate Brachytherapy - A Composite Analysis Model

Goetz ThI^{1,2*}, Tome AM³, Hensel B⁴, Bert Ch² and Lang EW¹

¹CIML, Biophysics, University of Regensburg, 93040 Regensburg, Germany

²Department of Radiation Oncology, University Hospital Erlangen Friedrich - Alexander University of Erlangen -
Nürnberg 91054 Erlangen, Germany

³IEETA, DETI, Universidade de Aveiro, 3810-193 Aveiro, Portugal

⁴Center for Medical Physics and Engineering, University of Erlangen-Nürnberg, 91052 Erlangen, Germany

ABSTRACT

Electromagnetic tracking (EMT) in high dose rate Brachytherapy has to face a number of signal processing challenges which we summarize in this study. We propose a coherent signal processing chain which encompasses a particle filter tracking of the state space trajectory of the sensors inside catheters implanted surgically into the breast of female patients. Singular spectrum analysis is employed to remove high amplitude artifact signals from the recordings as well as to decompose simultaneously recorded signals from additional fiducial sensors used to monitor breathing motions. Ensemble empirical mode decomposition is applied to both, the fiducial and solenoid sensor signals to decompose them into their intrinsic modes. Information-theoretic similarity measures serve to identify those intrinsic modes which carry information about the breathing mode contamination of the observed solenoid sensor signals. Finally, a multi-dimensional scaling achieves a common principal coordinate system where both, the various EMT signals and related data deduced from an initial X-ray CT imaging can be compared quantitatively to identify any deviations from the treatment plan established with the CT data. We also consider the distributions of such deviations and demonstrate their heavy-tailed character. A Hartigan dip test is employed to establish a uni- or bi-modal character of these distributions which we approximate by alpha-stable distributions.

Keywords: Electromagnetic tracking, Particle filtering, Singular spectrum analysis, Ensemble empirical mode decomposition, Hartigan dip test, Alpha-stable distributions

INTRODUCTION

Motivation

The treatment of female breast cancer involves a surgical intervention to remove cancerogenous tissue followed often by a radiation therapy. Recently, a variant of the latter, called high dose rate brachytherapy (HDR-BT) [1] has become increasingly popular. Thereby the tumor bed is irradiated with high radiation dose (up to 35 Gy) in short time intervals. The application of the radiation is achieved with a radioactive source, ¹⁹²Ir for example, which irradiates the tumor bed with 370 keV γ -photons. HDR-BT relies on the observation that recurrences following breast radiotherapy appear mostly at the tumor bed. The source is moved inside 14-20 catheters, which are inserted into the female breast by a surgical intervention following a design detailed by a medical expert. Most recently, a variant, called accelerated partial breast irradiation (APBI) [2,3] allows to apply even higher dose rates up to 50 Gy. Such high dose rates deposit large amounts of destructive energy and require an accurate placement of the radiation source for a precise delivery of the radiation energy. An ultimate constraint of the radiation treatment is to prevent healthy tissue from being irradiated erroneously. The latter requirement, however, puts stringent conditions to the positioning accuracy which, moreover, needs to be maintained during the treatment period which usually extends over roughly one week. As during this period the patients are moving freely, such a constraint seems unrealistic in clinical practice. Anyway, based on the CT-image, a treatment plan is established which determines the number of dwell positions of the radioactive source

as well as its related dwell times [4,5]. By varying dwell position and dwell time, a complex dose distribution in the target volume can be delivered individually.

The establishment of a treatment plan is based on an X-ray computed tomography (CT) image which is acquired shortly after the surgical implantation of the catheters. With this image the spatial position of the inserted catheters is determined relative to the anatomy of the patient. Because of the patient movement between the treatment sessions, and a possible tissue swelling (edemas) after the surgical intervention, the precise spatial positioning of the various catheters needs to be controlled each time when a radiation treatment session is intended. Measuring the spatial positions of the catheters can be achieved with an electromagnetic tracking system (EMT) where a field generator is placed over the patient's breast and solenoid sensors are moved inside the catheters according to the treatment plan to measure the spatial locations of the dwell positions. Because the field generator is placed in each session differently relative to the female breast, each measurement session refers to a different coordinate system. Hence the question arises, how one can map these different data to a common coordinate system to render them comparable quantitatively. A common solution is to externally register, usually by optical techniques, the position of additional markers, and to estimate the corresponding coordinate transformations to map all measurements to a common coordinate system.

This survey discusses a complete signal processing chain for the analysis of EMT data collected during an HDR-BT and summarizes our recent efforts in this field [6-8]. Especially, it pursues the possibility to reconstruct catheter shapes and positions and the related source or sensor dwell positions from EMT measurements alone without recourse to fiducial sensors. An alternative method based on a coherent point drift (CPD) algorithm has been proposed recently [9-12]. Thus by relying only on EMT measurements, the key difficulty arises from the fact that during the treatment the FG has to be removed and repositioned several times to either manually or with a remote after loader insert the radiation source or the sensor into the catheters. Hence, every new determination of catheter position and source dwell position refers to a different coordinate system rendering the reference data determined initially via X-ray CT-imaging obsolete. A way out of this dilemma is proposed here by considering only distances between dwell positions and applying multi-dimensional scaling to estimate dwell position coordinates within a common coordinate system. Furthermore, employing only EMT measurements while monitoring the sensor motion inside the catheters with the breathing motion overlaid, fiducial markers are usually placed on the chest of the patient to monitor the position of the breast relative to the field generator. If patients are breathing, and even talking, during the EMT measurements, the trajectory of the solenoid sensor consists of a, possibly non-linear, superposition of the movement inside the catheters and the actual breathing motion. Hence, this breathing artifact needs to be removed from the EMT recording without disturbing the sensor tracks inside the catheters. In this study, artifact removal will be achieved by applying singular spectrum analysis (SSA) as well as ensemble empirical mode decomposition (EEMD). But even if this could be achieved, the sensor positions are still not perfect due to measurement noise and additional noise contributions. Hence strategies based on particle filters are proposed here to achieve a precise description of the actual states of the sensors inside the catheters during the EMT measurements. These state space trajectories perfectly monitor the spatial positions and orientations of these catheters and their deviations from the treatment plan.

In summary, the current study presents a coherent and thorough expert system by putting together some very recent efforts to deal with data analysis aspects concerning electromagnetic tracking of solenoid sensor positions inside catheters implanted into female breasts within a high dose rate brachytherapy. It summarizes related work which dealt with specific aspects of the proposed data analysis methodology, namely particle filtering, multidimensional scaling and some aspects of automatization of the data analysis. It presents a coherent expert system thoroughly describing the complete signal processing chain, thus rendering it an expert system for practitioners who have to deal with EMT data collected during an HDR-BT.

Related works

In brachytherapy, new catheter and applicator technologies considerably improve accuracy, efficiency, and treatment outcomes [1,2]. Sensor and radiation source positions inside catheters are mostly located using imaging techniques [13-15]. However, they are hampered with limitations in catheter reconstruction. This triggered the development of Electromagnetic Tracking (EMT) systems [16-19] for an automatic tracking of sensor positions inside catheters. An EMT system provides data relative to the coordinates of the field generator, i.e., on CFG. The latter have to be transformed to the treatment planning coordinate system CTPS. This transformation is highly anisotropic and is mostly based on a rigid-body, point-based registration via fiducial sensors with positions known in both coordinate systems through optical measurements [20,21]. This combination of EMT and imaging system yields errors in catheter reconstruction much larger than corresponding intrinsic EMT tracking errors [1]. A recent review [12] summarizes the use of EMT for treatment verification in brachytherapy. By nature, EMT systems are highly susceptible to

distortions, based on nearby metal parts, of the magnetic field produced by the field generator. To alleviate such distortions, calibration procedures performed in a fixed environment and preparatory measurements are needed [22]. A calibration procedure for dynamic field distortion compensation has also been discussed recently by Sadjadi et al. [23]. General limitations of EMT systems, their accuracy and noise performance are discussed by Zhou et al. [1] and quality assurance aspects as well as catheter technology and reconstruction accuracy are discussed in recent reports by Franz et al. [16]. A recent study avoided external registration and reports the use of an iterative closest point algorithm employing a finite difference method to compare catheter reconstruction results from both conventional CT and EMT. Unfortunately, the performance of EMT systems is mostly assessed with ideal, undistorted laboratory settings, but corresponding data from a clinical BT treatment environment are almost non-existent [1,10,12]. The current study presents for the first time a coherent signal processing chain which allows to automatically analyze EMT data during an HDR-BT and which was shown to work well with data collected with patients in a clinical environment [24].

SIGNAL PROCESSING CHAIN

For the analysis of EMT data sets, acquired during HDR-BT, Multi-Dimensional Scaling (MDS) [25-27] deems appropriate to render comparable dwell position determinations of sensors during a full radiation treatment cycle. However, even then the estimated coordinates are inevitably contaminated with measurement noise, contributions from random catheter displacements during tissue swelling and patient movement between the treatment sessions, and, last but not least, periodic disturbances due to breathing. To unravel such noise contributions and to identify the undistorted dwell positions of the sensors moving inside the catheters, particle filter (PF) tracking [28,29] is employed here and applied as a first step of the signal processing chain. This is then followed by a Singular Spectrum Analysis (SSA) for outlier removal and subsequent ensemble empirical mode decomposition (EMD) for breathing artifact identification and removal. Next the simultaneously recorded EMT signals from the fiducial sensors are decomposed with SSA as well. Figure 1 illustrates the effect of using the fiducial sensor signal as reference to identify the intrinsic mode representing the breathing mode contribution to the tracked EMT signal. During reconstruction, this breathing mode contribution can be omitted yielding an artifact-free sensor signal as is illustrated in Figure 1. Such undistorted sensor trajectories, mirroring catheter shapes, ideally, should be in perfect agreement with the treatment plan. If not, any deviations can be quantified employing the statistical tools discussed later on. Possible error sources can then be identified early enough to be corrected or for the treatment plan to be adapted. The currently proposed protocol thus combines a plethora of machine learning tools to enable the practitioner of using only intrinsic EMT measurements of spatial positions of the solenoid sensors for catheter reconstruction and treatment plan verification.

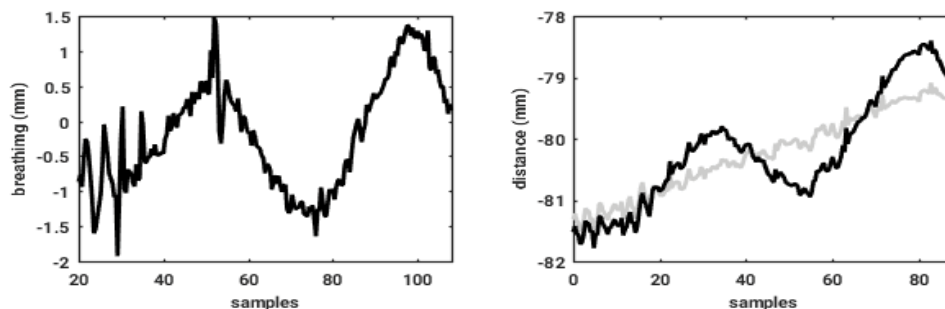


Figure 1: Left: Mean breathing signal recorded by the fiducial sensors. Right: Tracked signal (black) and tracked signal after removing the breathing artifact with EEMD (gray)

The main ingredients of the method

The complete signal processing chain is illustrated in Figure 2. It encompasses the following processing steps:

PF The measured sensor signals are ballasted with measurement noise. To estimate the sensor state during the sensor's motion inside a catheter, we propose to employ a particle filter [7] to estimate the unobservable sensor state from the noise contaminated observation of the dwell positions provided by the EMT system. The construction of the state evolution model needs prior knowledge about the original dwell positions as manifested in the treatment plan. Furthermore, additional knowledge about the superimposed breathing motion is needed to be entered into the state evolution model as well. Last but not least, large amplitude artifacts from an occasional malfunctioning of the measurement device need to be removed to yield an undistorted state space trajectory. These goals are achieved with the steps of the processing chain described next.

SSA While relying only on EMT measurements, fiducial sensors are placed on the chest of the patient to monitor the breathing motion which superimposes onto the recorded EMT sensor signals registering the sensor movement

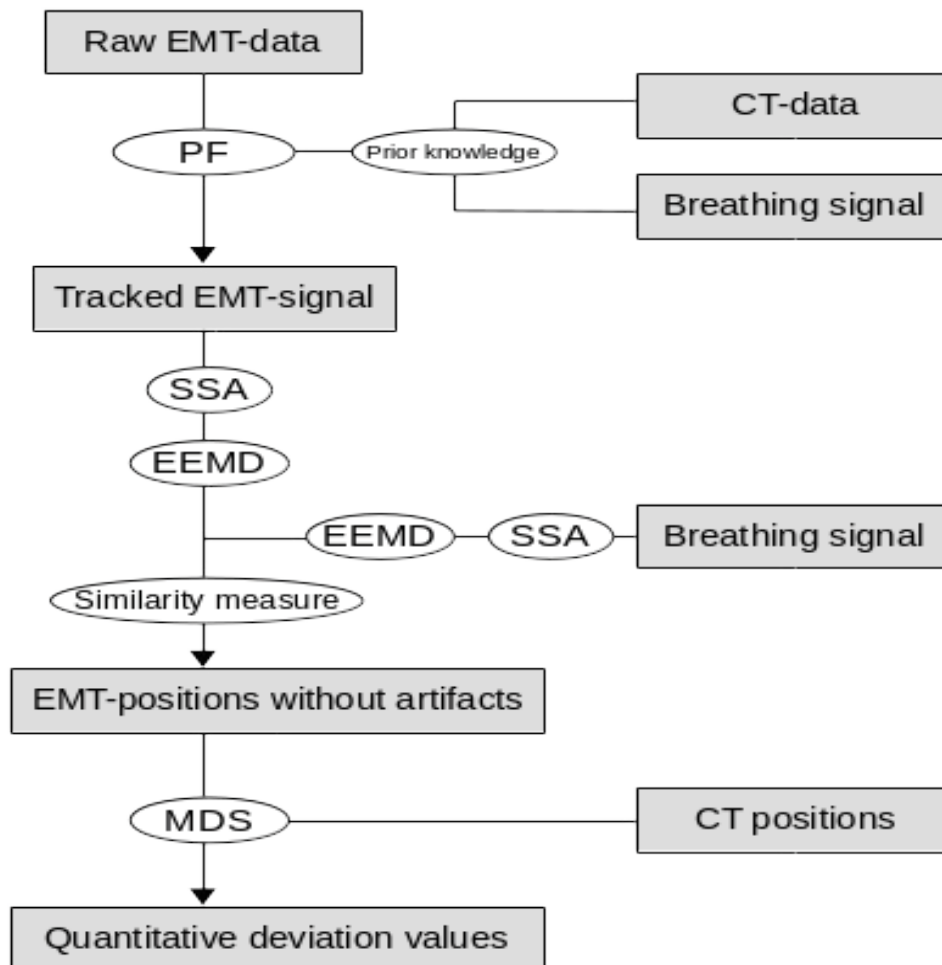


Figure 2: The signal processing chain of the proposed method

inside the catheters. This breathing signal is decomposed employing a singular spectrum analysis (SSA) [30,31] which already showed good performance in removing artifacts from electroencephalographic recordings of brain signals [32,33]. In addition to noise contributions to the fiducial breathing signal, high amplitude artifacts due to malfunctioning of the measurement device are observed regularly and can be removed reliably with SSA as well as will be shown in this study.

EEMD Given then a noise-reduced and artifact-free breathing signal, we need to remove its contribution to the measured EMT sensor signals without distorting the latter. As we have shown in a recent study [7], this can be achieved robustly by applying an ensemble empirical mode decomposition (EEMD) [34-37]. The latter is employed to decompose both an average signal from the fiducial sensors as well as the signals from the solenoid sensor into intrinsic modes which are separated according to their characteristic time/frequency scales. Note that breathing signals may encompass components stemming from occasional motions of patients lying on the bench during the EMT measurement session. Also note that if patients are speaking during the sessions, their breathing signals can become quite complex and irregular. The challenge here is to design a signal evaluation procedure which allows to automatically, i.e., without user intervention, removing such breathing artifacts from the EMT sensor signals.

MDS In a recent study [6] we pursued the idea of reconstructing the positions of all catheters purely from CT and EMT measurements without recourse to externally measured reference points. The proposal was to solely rely on relative distances which are shift invariant. The suitable mathematical technique is called multi-dimensional scaling (MDS) [25,27] which shows an equivalence between normalized distance matrices and related kernel matrices, both of which represent symmetric, real-valued matrices for which an eigendecomposition exists. Hence the related eigenvectors span the sought for common coordinate system which allows a quantitative characterization of any spatial deviation

of a dwell position of a sensor inside a catheter from its CT-based dwell position prescribed in the treatment plan. Any deviations can then be characterized statistically as will be explained later on as well.

In the following we discuss the theoretical background behind these techniques and explain how they should be integrated into the signal processing chain to form a convenient and powerful analysis tool for EMT data collected during a HDR-BT.

Particle filter for sensor tracking

Bayesian filtering

EMT measurements of the spatial dwell positions of a sensor moving inside a catheter represent, at discrete times tm , noisy observations $z_m^{(k,r)}$, $k = 1, \dots, K$; $r = 0, \dots, R$ of an underlying but unobservable state space trajectory $X_{1:m}^{(k,r)}$, formed by a sequence of latent states $X_m^{(k,r)}$. Here $k \in [1, K]$ denotes the number of catheters and $r \in [0, R]$ counts the number of sessions whereby $r=0$ denotes the data set obtained from the X-ray CT image and $r=1, \dots, R$ denote the EMT data sets.

Sequential Monte Carlo sampling techniques [28,38,39] also called Particle Filter, are frequently used in such state space estimation problems. They approximate the posterior density by a set of random samples, called *particles* X_m^p , with associated weights W_m^p [7,29]

$$p(x_{0:m} | \mathbf{z}_{1:(m-1)}) \approx \sum_{p=1}^P W_m^p \delta(x_{0:m} - X_{0:m}^p)$$

Statistics can now be estimated based on these samples and weights, and for $P \rightarrow \infty$ this Monte Carlo representation approaches an optimal Bayesian estimate of the posterior probability density.

Latent state estimates are based on a physical model of the dynamical system (state evolution model) $f(x_m, \varepsilon_m^{(x)})$ given the measurements $\mathbf{Z}_{1:m}$, represented by an observation model $h(x_m, \varepsilon_m^{(m)})$ where, $\varepsilon_m^{(x)}$ denotes the state noise and $\varepsilon_m^{(m)}$ the measurement noise, respectively. Hence we have a state evolution model.

$$p(x_m | x_{m-1}) \leftrightarrow x_m = f(x_m, \varepsilon_m^{(x)})$$

- an *observation model*, given a state estimate x_m

$$p(z_m | x_m) \leftrightarrow z_m = h(x_m, \varepsilon_m^{(m)})$$

Thus during the iterations, the *filtering density* $p(x_m | \mathbf{z}_{1:m})$ can be obtained from repeated predictions of the state evolution model

$$p(x_m | \mathbf{z}_{1:(m-1)}) = \int p(x_m | x_{m-1}) p(x_{m-1} | \mathbf{z}_{1:(m-1)}) dx_{m-1}$$

- repeated *updates* of the *observation model*

$$p(x_m | \mathbf{z}_{1:(m-1)}) \propto p(z_m | x_m) p(x_m | \mathbf{z}_{1:(m-1)})$$

Such sequential Monte Carlo methods (particle filters) can be applied to non-linear dynamical models with non-Gaussian error distributions [40] (Figure 3).

State evolution and observation models

The particle filter needs as input a *state evolution model* as well as an *observation model*. Both are explicated in the following for applications to the analysis of EMT data from a HDR-BT. The state evolution model consists of three parts concerning the sensor movement inside the catheter, the superimposed breathing motion and some noise contributions. For the observation model the simplest possible ansatz is chosen.

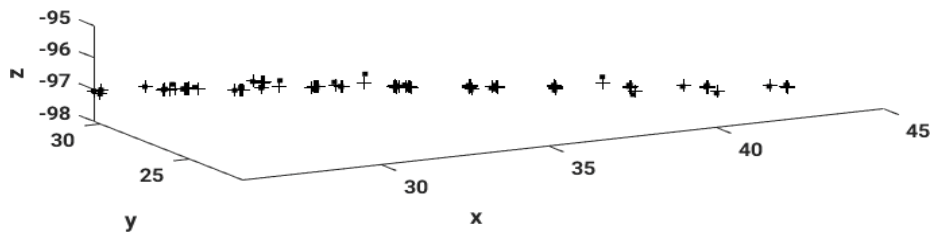


Figure 3: EMT-measured data (dots) and corresponding particle filter estimates (crosses)

State evolution model

Based on the CT-image slices, a treatment plan is designed which provides all dwell positions of the sensor in all implanted catheters. In addition, for each dwell position its distance to the very end of the catheter is known. During the EMT control measurements, sensor trajectories are tracked electromagnetically and result in noisy versions of the underlying true sensor states which, however, can be estimated employing a particle filter as is demonstrated in Figure 3.

The state evolution model can be deduced from the CT measurements, which refer to the CT coordinate system, however. After transformation to the EMT co-ordinate system and accounting for the dependence of the sensor positions on the superimposed breathing motion and other time-dependent distortions, the model finally yields.

$$\begin{aligned}
 f(l_m, t) &= f_1(l_m) + f_2(t) + \varepsilon_f \\
 &= R \cdot f_{1CT}(l_m) + S + f_2(t) + \varepsilon_f \\
 &= R \cdot A \cdot L + S + a/2 + \sum_{q=1}^7 (b_q \cdot \cos(\omega_q \cdot t) + c_q \cdot \sin(\omega_q \cdot t)) + \varepsilon_f
 \end{aligned}
 \tag{1}$$

Where, $a, b_q, c_q \in R^3$. Note that for simplicity the breathing mode contribution $f_2(t)$ is approximated by a Fourier series of order seven (Figure 4).

After the sensor positions have been tracked by the particle filter, artifact and breathing mode contributions to the trajectory will be removed with more sophisticated methods based on singular spectrum analysis (SSA) or an ensemble empirical mode decomposition (EEMD).

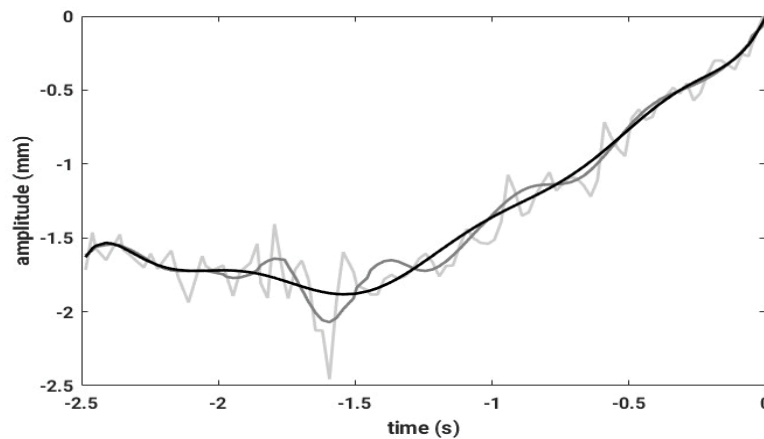


Figure 4: The original EMT sensor signal is shown in bright grey, its noise-reduced variant is exhibited in dark grey and the tracked state space trajectory is illustrated in black

Observation model

For the observation model h the simplest possible choice is an identity plus a normally distributed measurement noise yielding.

$$h(l, x, y, z, t_m) = \begin{pmatrix} l_m \\ x_m \\ y_m \\ z_m \\ t_m \end{pmatrix} + \varepsilon_f$$

A resampling scheme

The particle filter (PF) approximates the posterior density, $p(\mathbf{x}_{0:m} | \mathbf{z}_{1:m})$, or its related filtering density $p(\mathbf{x}_m | \mathbf{z}_{1:m})$, by a weighted set of particles $\{\mathbf{x}_{0:m}^p, w_m^p\}_{p=1}^P$. Hence, it generates and evaluates P different trajectories by directly updating the Bayesian recursion relations at each iteration. Employing importance sampling from the state transition density as proposal density, i.e.,

$$q(\mathbf{x}_{0:m} | \mathbf{z}_{1:m}) = q(\mathbf{x}_m | \mathbf{x}_{0:(m-1)}, \mathbf{z}_{1:m})q(\mathbf{x}_{0:(m-1)} | \mathbf{z}_{1:(m-1)}) \tag{2}$$

combined with the *Markov* assumption yields:

$$q(\mathbf{x}_m | \mathbf{x}_{0:(m-1)}, \mathbf{z}_{1:m}) = q(\mathbf{x}_m | \mathbf{x}_{(m-1)}) \tag{3}$$

Sampling new particles from this proposal density results [41]

- a particle update

$$p(\mathbf{x}_{0:m}^p | \mathbf{z}_{1:(m-1)}) = W_{m-1}^p p(\mathbf{x}_m^p | \mathbf{x}_{m-1}^p) X^{(p)} \sim p(\mathbf{x}_m | \mathbf{x}_{m-1}) \tag{4}$$

- and a weight update

$$\begin{aligned} W_m^{(p)} &= W_{m-1}^{(p)} p(z_m | \mathbf{x}_m^{(p)}) \\ W_m^{(p)} &\propto p(z_m | \mathbf{x}_m^{(p)}) \end{aligned} \tag{5}$$

Finally, the weights $\{w_m^p\}_{p=1}^P$ are normalized to sum to one (Figure 5).

In summary, the processing chain results in the sampling importance resampling (SIR) algorithm [42] which uses the state transition distribution $p(\mathbf{x}_m | \mathbf{x}_{m-1}^p)$ as proposal density and applies re-sampling at every iteration. It can be summarized in the following steps [29], as applied to the system evolution from t_{m-1} to t_m :

Step 1: For $p=1, \dots, P$ draw new particles \mathbf{x}_m^p from the importance density by employing the transition model

$$q(\mathbf{x}_m) = \sum_{p=1}^P w_{m-1}^p p(\mathbf{x}_m | \mathbf{x}_{m-1}^p)$$

To do so, choose a random number r uniformly from $[0, 1]$ and choose particle $p=r$, then sample from the prior density $p(\mathbf{x}_m | \mathbf{x}_{m-1}^p)$.

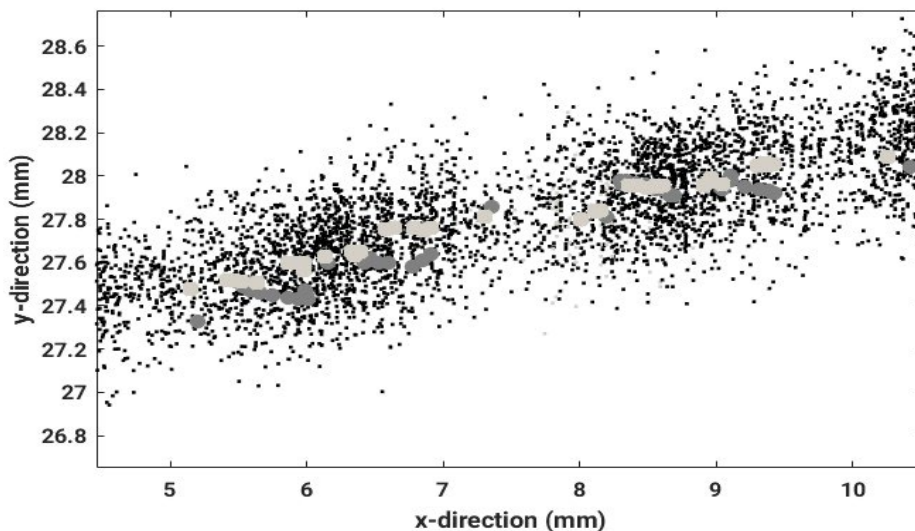


Figure 5: The x, y - coordinates of the measured EMT dwell positions (dark gray) are compared to particle filter estimates (black) (out of 20000 sampled particles per time step only 100 are shown for visualization purposes). The resulting positions are colored with bright gray dots

– Use the corresponding likelihood to calculate corresponding weights:

$$w_m^p = p(z_m | z_m^p)$$

The samples x_m^p are taken from $w_m^p = p(x_m | z_{1:m-1})$ and re-weighting them accounts for the evidence of the observations z_m .

Step 2: Calculate the total weight $w_m = \sum_{p=1}^p w_m^p$ and normalize the particle weights:

$$w_m^p = w_m^{-1} w_m^p \forall p = 1, \dots, p$$

Step 3: Re-sample the particles by doing the following:

– Compute the cumulative sum of weights

$$w_m^p = w_{m-1}^p + w_m^p; \forall p = 1, \dots, p, w_m^0 = 0$$

– Let $p=1$ and draw a starting point u_1 from a uniform distribution $U(0, P^{-1})$

– For $p'=1, \dots, P$ do the following

- move along the cumulative sum of weights by setting $u_p' = u_1 + P^{-1}(p'-1)$
- while $u_p' > W^p$ set $p=p+1$
- assign samples $x_m^{p'} = x_m^p$
- assign weights $w_m^{p'} = P^{-1}$

This resampling procedure avoids having many degenerate particles with vanishing weights. However, it can lead to a loss of diversity as the resulting samples may contain many redundant particles. This sample impoverishment is often observed in case of small process noise.

Artifact removal

After the sensor state dynamics has been tracked by particle filtering, the resulting EMT sensor signal still contains artifacts stemming from device malfunctioning and breathing modes. The following subsections will describe how such artifacts can be removed employing singular spectrum analysis and empirical mode decomposition.

Singular spectrum analysis

After having tracked the sensor dwell positions with the particle filter, the resulting trajectory still contains large amplitude artifacts (outliers) and the breathing mode contribution. The former are due to occasional malfunctioning of the measurement device. Because of the large amplitude of outliers, singular spectrum analysis (SSA) techniques [43] deem most appropriate to decompose the recorded non-stationary time series and remove such artifacts from the EMT recordings. Furthermore, an independent measure of the breathing mode is obtained from an EMT recording of three 6 DoF fiducial sensors fixed to the chest of the patient. This signal is also decomposed with an SSA, and only the dominant principal component is retained for further processing aiming at removing the breathing mode contribution to the sensor trajectory as obtained from the particle filter (Figure 6).

Singular Spectrum Analysis (SSA) is a well-known signal analysis technique to decompose the original time series into a sum of orthogonal components. Most of them have an immediate interpretation as trends, structure less white noise or oscillatory components [30,31,33].

Let $x(t) = (x(t_1) \dots x(t_T))^{\text{AT}} \equiv x_t = (x_1 \dots x_T)^{\text{AT}}$ represent a zero mean sensor signal with total length T . After selecting an embedding dimension E and a proper segment length $L \ll T$ such that $T = E + L - 1$, we have $x_e = (x_e, \dots, x_{e+(L-1)})T$. Any analysis of such a time series with SSA requires two steps [43]:

- A decomposition step, which encompasses embedding of the time series into E delayed coordinates combined with an Eigendecomposition of a correlation matrix, and
- A reconstruction step, which encompasses anti-diagonal averaging and reverting the embedding.

SSA is used in this data processing chain to remove large amplitude artifacts from solenoid sensor signals measured with EMT. Typically, such artifacts dominate the signal decomposition and correspond to the principal mode related with the largest Eigenvalue as is shown in Figure 6.

Ensemble empirical mode decomposition

An independent measure of the breathing mode is obtained from an EMT recording of three 6 DoF fiducial sensors

fixed to the chest of the patient. After SSA decomposition, the principal component corresponding to the largest Eigenvalue serves as a reference signal to which the intrinsic modes resulting from an Ensemble Empirical Mode Decomposition (EEMD) need to be compared to identify those modes which contain information about the breathing mode artifact (Figure 7).

An EEMD [34-37,45] represents a noise-assisted analysis technique of non-stationary and non-linear time series, which results in a list of J oscillatory components with characteristic time scales τ_j ordered with increasing period, i.e., decreasing local frequency. It locally decomposes any non-stationary time series in a sum of intrinsic modes (IMFs), which represent zero-mean amplitude- and frequency-modulated components. A flowchart of the EEMD algorithm is given in Figure 7, while Figure 8 exemplifies the decomposition of the signal shown in Figure 4 already.

In short, EEMD proceeds as sketched in Figure 7 [46,47]. After EMT sensor signal recording, denoising and particle filtering, the tracked sensor signal still contains the breathing artifact. The latter can be removed by decomposing the signal with an EEMD (Figure 8) and identifying the intrinsic mode which best represents the breathing mode as reflected by the average fiducial sensor signal. Tracked EMT signal reconstruction while omitting the contribution from the intrinsic breathing mode yields an uncontaminated sensor signal which nicely mirrors the related catheter shape as can be seen from Figure 9.

With patients speaking during EMT signal recording, the tracked sensor signals become very complex and breathing mode artifact removal via EEMD needs to be iterated until the artifact is suppressed sufficiently as is illustrated in Figure 9.

Similarity measures

The data processing chain encompasses an EEMD decomposition of the fiducial and the solenoid sensor signals, respectively [7]. This decomposition aims at identifying those intrinsic mode(s) which most closely resemble the breathing mode artifact. During signal reconstruction, these intrinsic modes will be neglected to reconstruct an artifact-free sensor signal. To achieve this goal, proper similarity measures are needed to automatically identify corresponding intrinsic modes of the fiducial sensor and the solenoid sensor signals, respectively. Hence several alternative measures of similarity can be applied to the decomposed sensor signals.

One of the most frequently employed similarity measures between two data sets considers a point-wise, linear correlation between stochastic variables which follow a normal distribution. The most popular correlation measure is the Pearson Correlation Coefficient (PCC) [48]. Given two time series segments with size $L \leq T$, $x=(x_1 \dots x_L)^T$ and $y=(y_1 \dots y_L)^T$, represented as vectors in an L -dimensional space, the Pearson correlation coefficient PCC is defined as:

$$PCC(x, y) = \frac{L \sum_{i=1}^L x_i y_i - (\sum_{i=1}^L x_i)(\sum_{i=1}^L y_i)}{\sqrt{L \sum_{i=1}^L x_i^2 - (\sum_{i=1}^L x_i)^2} \sqrt{L \sum_{i=1}^L y_i^2 - (\sum_{i=1}^L y_i)^2}} \quad (6)$$

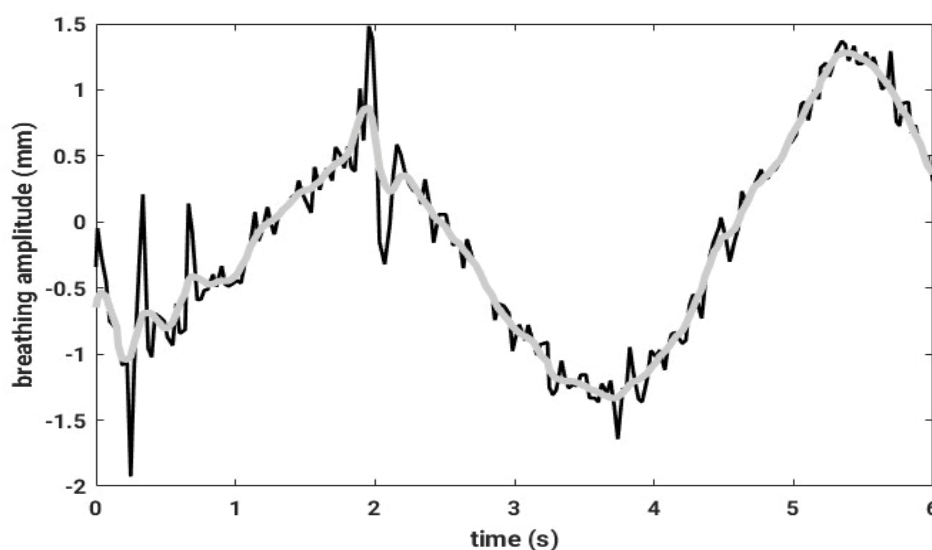


Figure 6: The breathing signal, obtained as an average of measured 6 DoF fiducial sensor signals, is shown in black, while in gray color the principal component resulting from an SSA is depicted

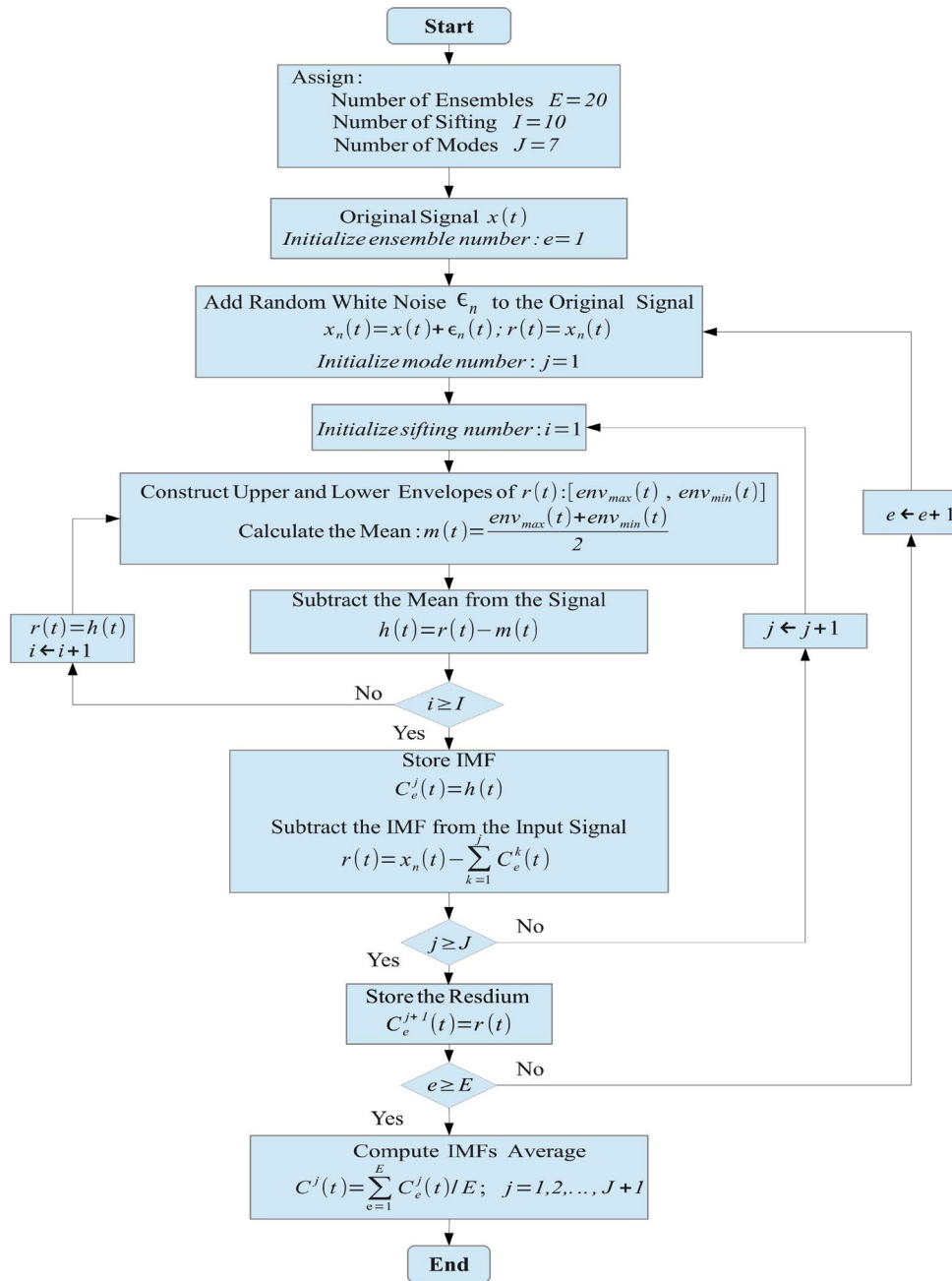


Figure 7: A schematic of the signal processing chain of an EEMD algorithm

If non-linear correlations apply, similarity measures should be based on similarities of distributions of the variables in the data sets. Such “metrics” are generally based on the Shannon entropy [49-51] and its related mutual information as well as on several divergences derived from it, as there is:

The Kullback-Leibler divergence (KLD) [52] or relative entropy is a non-symmetric measure of similarity between two distributions P and Q .

$$D_{KL}(X \parallel Y) \equiv D_{KL} \sim (p(X) \parallel q(y)) = \sum_{l=1}^L p(\hat{x}_l) \ln \left(\frac{p(\hat{x}_l)}{q(\hat{y}_l)} \right) \tag{7}$$

Where, the stochastic variables need to be normalized according to,

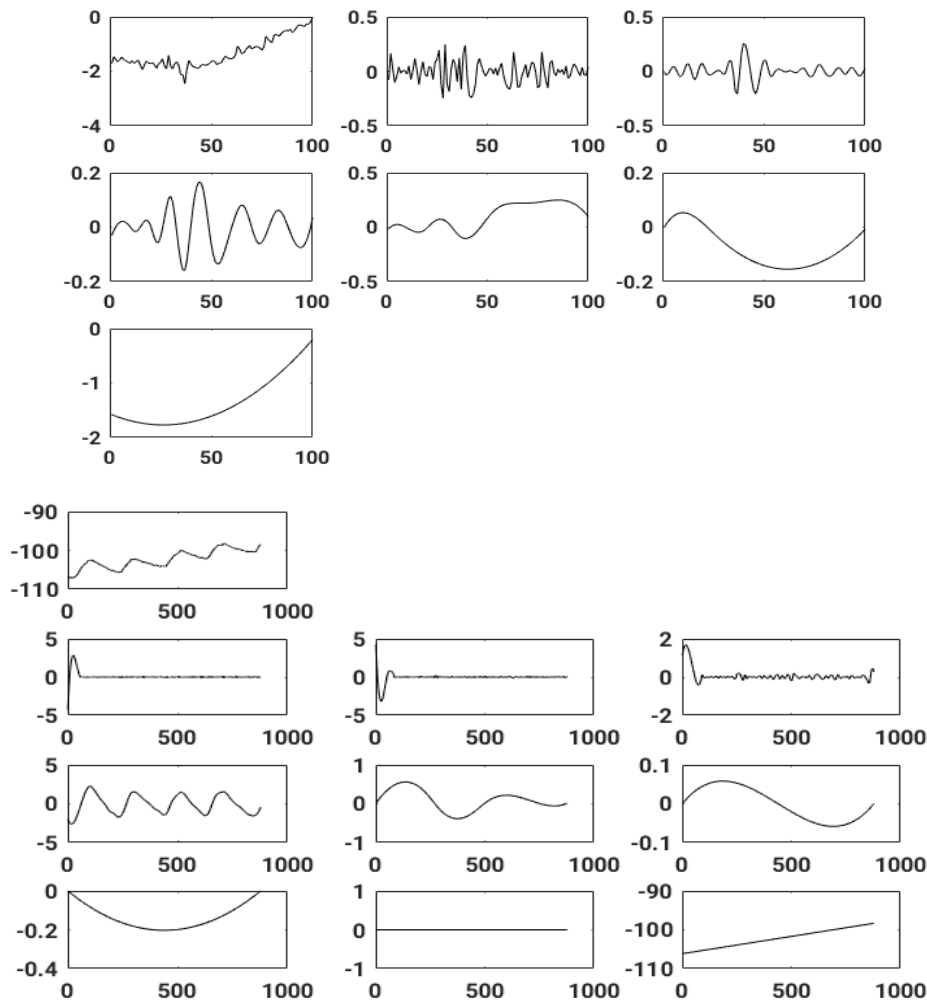


Figure 8: Top: The top row shows an EMT signal segment, which contains a high amplitude artifact. The following two rows show the corresponding intrinsic modes ordered from top left to bottom right with decreasing frequency. Bottom: The top row presents a tracked signal, which exhibits a prominent breathing mode contribution. The following two rows present the related intrinsic modes ordered from top left to bottom right with decreasing frequency. In IMF 4, 5 and 6 (bottom row), the breathing motion is contained with IMF 4 providing the dominant contribution.

$$\hat{Y}_l = \frac{y_l}{\sum_{l=1}^L y_l} \quad \hat{x}_l = \frac{x_l}{\sum_{l=1}^L x_l} \quad \text{and} \tag{8}$$

It can be understood as the loss of information if $p(x)$ is modeled by means of $q(y)$.

The Jensen–Shannon divergence (JSD) [53,54] is a symmetrized and smoothed version of the KLD and the square root of the Jensen–Shannon divergence is a metric often referred to as Jensen-Shannon distance $d_{JS} = \sqrt{JSD}$.

- Consider two realizations $p(x), q(y)$ of discrete probability distributions P, Q . The $JSD(P||Q)$ then is defined as:

$$JSD(P || Q) = \frac{1}{2} D_{kl} \left(p || \frac{1}{2}(p+Q) \right) + \frac{1}{2} D_{kl} \left(Q || \frac{1}{2}(p+Q) \right) = H \left(\sum_{n=1}^N w_n p_n \right) - \sum_{n=1}^N w_n H(p_n) \tag{9}$$

Where, for the second equality, $N=2, P \equiv P1, Q \equiv P2$ is used and $w1=w2=1/2$. Thus, the JSD measures the similarity of each of the two considered distributions with their corresponding mixture distribution.

A comparison of the impact of these different similarity measures onto the reconstruction quality of sensor dwell positions reveals that all yield quite similar results with differences less than the measurement precision as is illustrated in Figure 10. Included in this comparison is the judgment of a human expert.

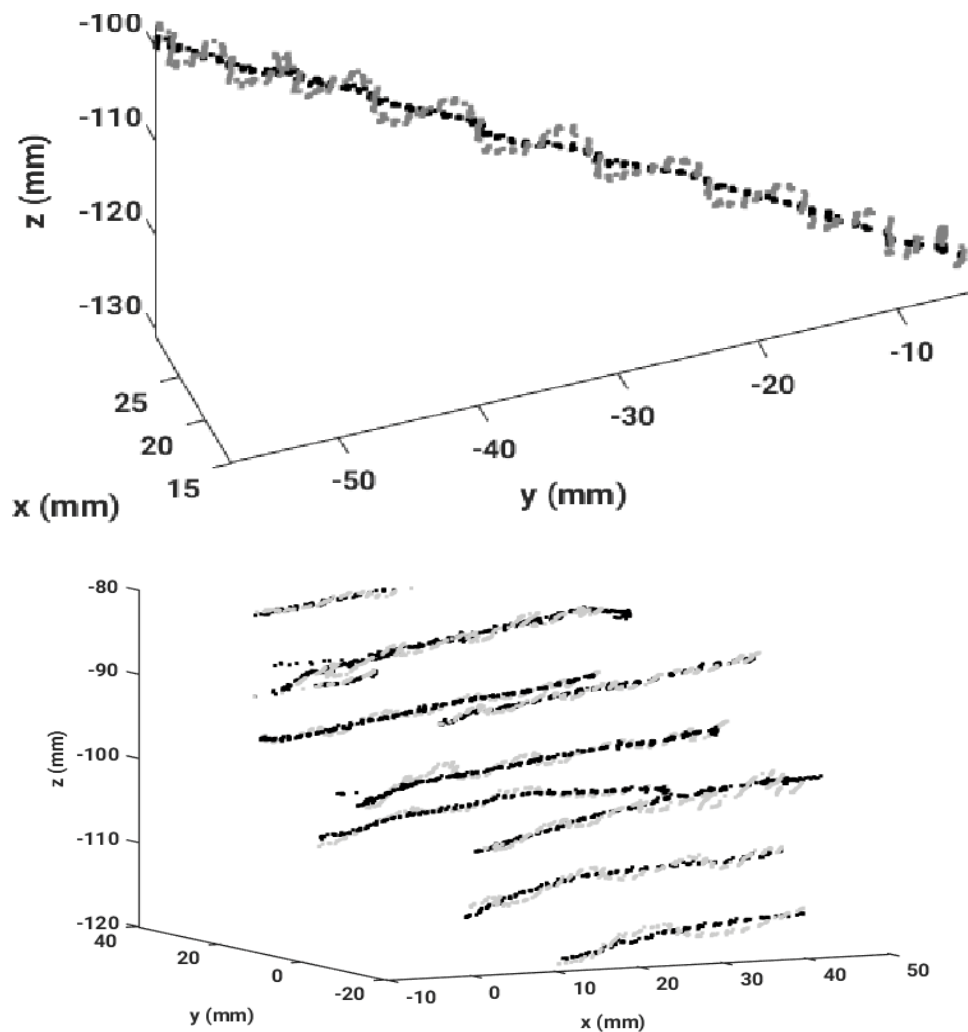


Figure 9: Top: Raw EMT data of one catheter (grey) including breathing mode distortions and the reconstructed data (black). The dots represent the true dwell positions of the solenoid sensor inside the catheter. Hence the reconstructed sensor trajectory reflects the catheter shape very well. Bottom: A complete set of raw EMT data (grey) recorded from the dwell positions of the solenoid sensor inside all implanted catheters, and the reconstructed dwell position data perfectly reflecting the catheters' shapes (black)

Multidimensional scaling

After having tracked spatial sensor positions with particle filters and having removed artifact contributions to the measured signal, still sensor dwell positions cannot be compared easily as they refer to different coordinate systems if measured in different sessions, neither can they be compared to the dwell positions defined in the treatment plan. To achieve a quantitative measure of spatial deviations between sensor positions measured by the EMT system during one of the treatment sessions and the sensor dwell positions defined in the treatment plan, the following signal processing is proposed.

Without using fiducial sensors, the only reliable measure concerns the relative distance of catheters and dwell positions of the solenoid sensors. Hence, the expert system discussed here proposes the use of a statistical technique, called Multi-Dimensional Scaling (MDS) [25-27], based solely on distance information, to reconstruct sensor coordinates which best explain the observed distances. Note that the latter are shift-invariant; hence different coordinate systems do not cause adverse effects. Additionally, the new method provides histograms of dwell position deviations and related sufficient statistics which enable early detection of any critical state of the system indicating a concomitant stop of any ongoing radiation treatment. Also such distributions of dwell position deviations directly reveal and identify any errors occurring during the treatment relative to the treatment plan.

During HDR-BT treatment, the spatial position of the implanted catheters is checked via EMT of a 5-DoF sensor moved inside the catheters according to the treatment plan. The latter is established once based on X-ray CT image slices. Any catheter displacement during radiation treatment is hard to quantify reliably based on EMT data alone. This

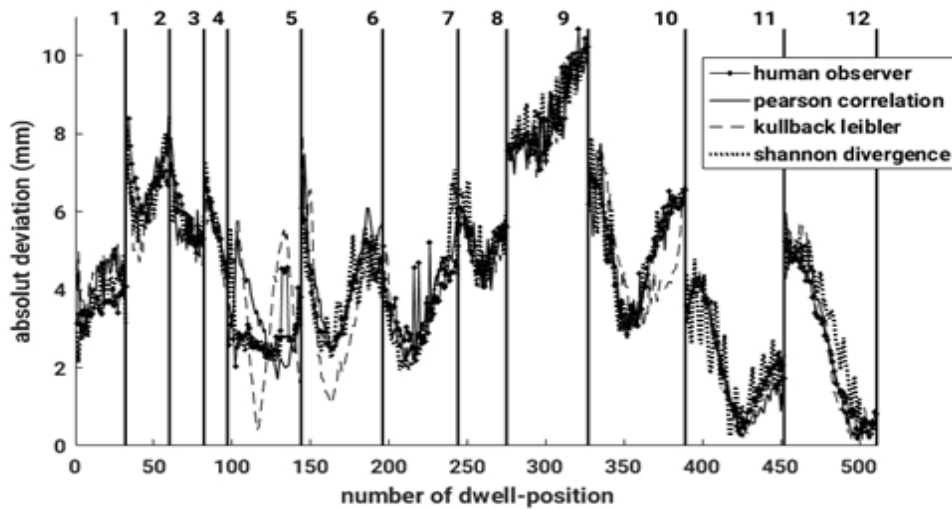


Figure 10: Absolute deviations for each pair of dwell positions (CT-EMT) are shown for four different reconstructed measurements. The black vertical lines mark the catheters

is a simple consequence of the fact that each EMT determination of the sensor positions in the course of the various treatment sessions refers to a different coordinate system due to patient movements and repeated field generator (FG) removal and re-positioning. The classical solution to this problem is an additional external registration, often by optical means. Recently we proposed an alternative solution relying solely on EMT data from the sensors and additional fiducial sensors fixed on the chest of the patient (Figure 11).

The latter were only employed to correct the breathing motion artifacts. This new method only considers distances between the actual sensor position and the one from the treatment plan. This set of distances is then taken to estimate a consistent set of coordinates which best describes all the distances observed during the test measurements. The solution is based on multi-dimensional scaling [26,27] which will be summarized in the following.

Given EMT data, the proposed method aims to quantify deviations of dwell positions as obtained from the EMT-measurements (EMT data set $X_{k,r}^{EMT}$) versus dwell positions obtained from the treatment plan (CT data set X_0^{CT}). Given M dwell positions defined in the treatment plan (CT data set), their three-dimensional coordinates can be collected as components of M column vectors $x_m = x_{1m}, \dots, x_{Nm}$, where $N=3, m=1$ and arranged in a data matrix X_0^{CT} :

$$X_0^{CT} = (X_1 \dots X_M) = \begin{pmatrix} x_{11} & \dots & x_{1M} \\ x_{21} & \dots & x_{2M} \\ x_{31} & \dots & x_{3M} \end{pmatrix} \tag{10}$$

Similar data matrices can be defined for all catheters during each control session and denoted as $X_{k,r}^{EMT}$ where the lower index k denotes the catheter and lower index r numbers the treatment sessions. Remember that the dwell positions of the sensors inside the catheters result from the proposed signal processing chain encompassing particle filter tracking, denoising and, finally, technical and breathing mode artifact removal via SSA and EEMD.

Dissimilarity matrix and kernel matrix

Metric multi-dimensional scaling (MDS) estimates a set of Cartesian coordinates which best explain a set of relative distances between measured spatial sensor positions [26]. Consider a distance matrix D_M of M dwell positions $x_m \in R^N$ in $N=3$ - dim space such that dissimilarities between pair-wise distances within point sets $X_{k,r}^{EMT}$ and X_0^{CT} , respectively are estimated as Euclidean distances of sensor positions according to:

$$(D)_{mm'} = -\frac{1}{2} d^2(x_m, x_{m'}) = -\frac{1}{2} (x_m, x_{m'})^T (x_m, x_{m'}) = -\frac{1}{2} (K_{mm} + k_{m'm'} - 2k_{mm'}) \tag{11}$$

Where, $k_{mm} = x_m^T x_m$, etc. denote entries to the related Kernel matrix. Thus, this metric measure of dissimilarity is transformed into a Kernel matrix representing inner products between vectors [55].

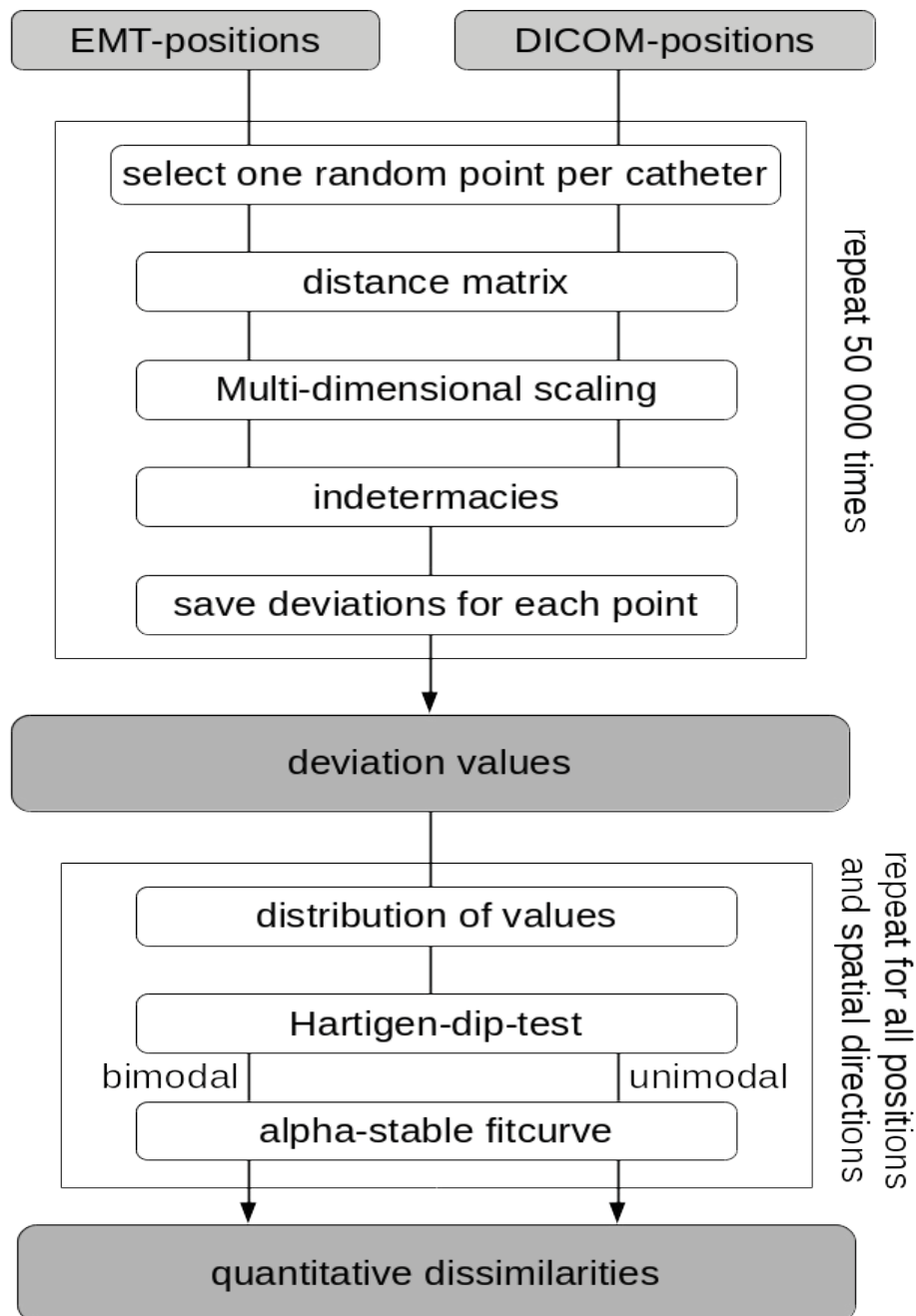


Figure 11: Flowchart of the MDS algorithm

Eigendecomposition of the distance matrix

Such a Kernel matrix is positive semi-definite, which the related dissimilarity matrix is not and its Eigendecomposition exists and can be achieved by principal component analysis (PCA) or singular value decomposition (SVD) [56].

MDS algorithm

In summary, the main steps of the MDS algorithm are the following:

Step 1 Build an $M \times M$ - dissimilarity matrix **D** from given distances between N -dim $x_m = (x_{1,m}, \dots, x_{N,m})^T$

Step 2 Double center the dissimilarity matrix using $O = I - \frac{1}{M} 11^T$ $D(c)=ODO$

Step 3 Estimates the SVD of $D^{(c)}$

$$D^{(c)} = K^{(c)} = \widehat{X}^T \widehat{X} = \left(\Lambda^{1/2} V^T \right)^T \left(\Lambda^{1/2} V^T \right)$$

Step 4 The set of M points, also called embedding, in $N=3$ - dim space are given in their spectral representation by the M columns of , i.e., $X_{nm} = \sqrt{\lambda_n} V_{nm}$, $n=1, \dots, N=3$; $m=1, \dots, M$

Note again, the MDS solutions are still indeterminate with respect to rotations and reflections while arbitrary translations, also called shifts, have been relieved by double-centering.

MDS analysis of measured dwell positions

As the interest here lies in estimating differences in dwell positions between each EMT measurement $X_{k,r}^{EMT}$ and its related X-ray CT recording $X_{k,r}^{EMT}$ differences in estimated spatial coordinates between all pairs of dwell positions from the CT data set (treatment plan) and any given EMT data set are computed. Thus, for each set of data matrices $X_{k,r}^{EMT}$, $D_{k,r}^{(c)}$ a distance matrix $D_{k,r}^{(c)}$ can be computed.

Knowing only these distance matrices, a consistent set of coordinates can be calculated by applying the MDS algorithm. As the latter is intimately related to eigenrepresentations of the corresponding Kernel matrices, the unique coordinate system is the principal coordinate system, spanned by the eigenvectors of the related co-variance matrix. Note that the MDS solutions are still not unique because of rotation and reflection indeterminacies. This issue can, however, be easily resolved by comparing the new coordinates, obtained from the MDS-algorithm of the CT data $\widehat{X}_{k,r}^{EMT}$, with the coordinates of the EMT data $\widehat{X}_{k,r}^{EMT}$. A possible center of gravity shift between the two sets of MDS coordinates is also taken into account. As a result, any catheter displacement in the course of the various treatment sessions can be quantified as deviations between the data sets $\widehat{X}_{k,r}^{EMT}$ and $\widehat{X}_{k,r}^{EMT}$, as is demonstrated in Figure 12. Such deviations are stored in an error matrix component-wise along each principal coordinate. For this study, the steps of the proposed MDS algorithm have been repeated 50000 times, resulting in roughly 5000 dwell position deviations. The histograms of these deviations are either mono- or bi-modal or show characteristics of heavy - tailed distributions. Thus, as we will show later, they can be represented by α -stable distributions. Following, some graphics illustrate the type of observations which we encountered in the course of the study. Considering Figure 12, certain dwell positions are encircled. Their corresponding histograms of deviations are identified as bi-modal by a *Hartigan Dip test*. In the projections of the dwell positions into the xy- and yz-plane of the PC axis system, a clear kink is seen in the respective dwell position trajectory, marking the onset of sudden and sizable deviations. This occurrence of small and large deviations in one trajectory causes the bimodal distribution of the corresponding histograms. The method is also very powerful in recognizing single catheter displacements during treatment. An especially bad example is shown in Figure 13, where quite a number of substantial catheter displacements (k3, k7 and k11) occurred. In addition, strong catheter bending happened (k2 and k12), and one catheter (k4) even had changed position during the course of the treatment cycle. Note that here and following all coordinates refer to the CT-axis system of the treatment plan (Figure 12).

On the contrary, Figure 13 exhibits only small deviations from the treatment plan except for one catheter (k15) which clearly underwent a pronounced shift during the course of the treatment. These few examples already illustrate the potential of the newly proposed method in quantitatively determining and visualizing any deviations of dwell positions from the treatment plan. And it is gratifying to see that similar results could be obtained with an independent method based on a coherent point drift technique [9,11] (Figure 13).

Statistics of dwell position deviations

The distribution of such deviations has been characterized further by studying the related histograms. Most frequently, uni-modal histograms are observed but occasionally also bi-modal histograms occur.

Hartigan dip test

A Hartigan dip test [57,58] is employed to estimate the probability of the data to follow an uni- or bi-modal distribution. Applying, the Hartigan Dip test to an error matrix of deviations, Figure 14 illustrates either the saturation of p-values at $p=1$ in case of an uni-modal histogram or their decline to zero in case of a bi-modal distribution (Figure 14).

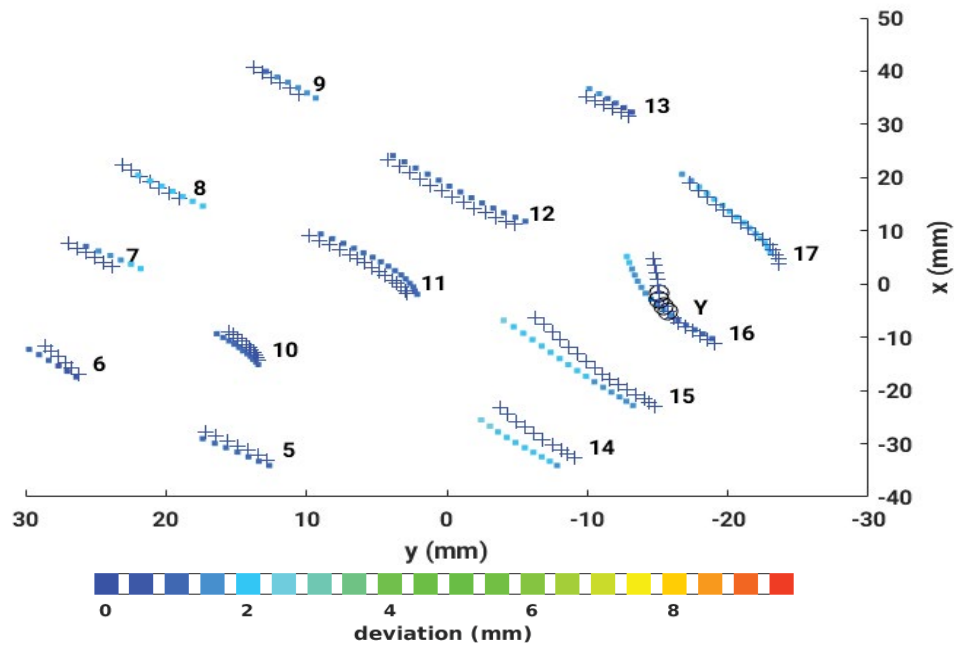


Figure 12: Reconstructed dwell positions inside the catheters projected into the x- y-plane. The CT data set is plotted with crosses, and the reconstructed EMT data set with colored circles. The colors are encoding the absolute deviations between the CT and EMT dwell positions, and correspond to the color bar

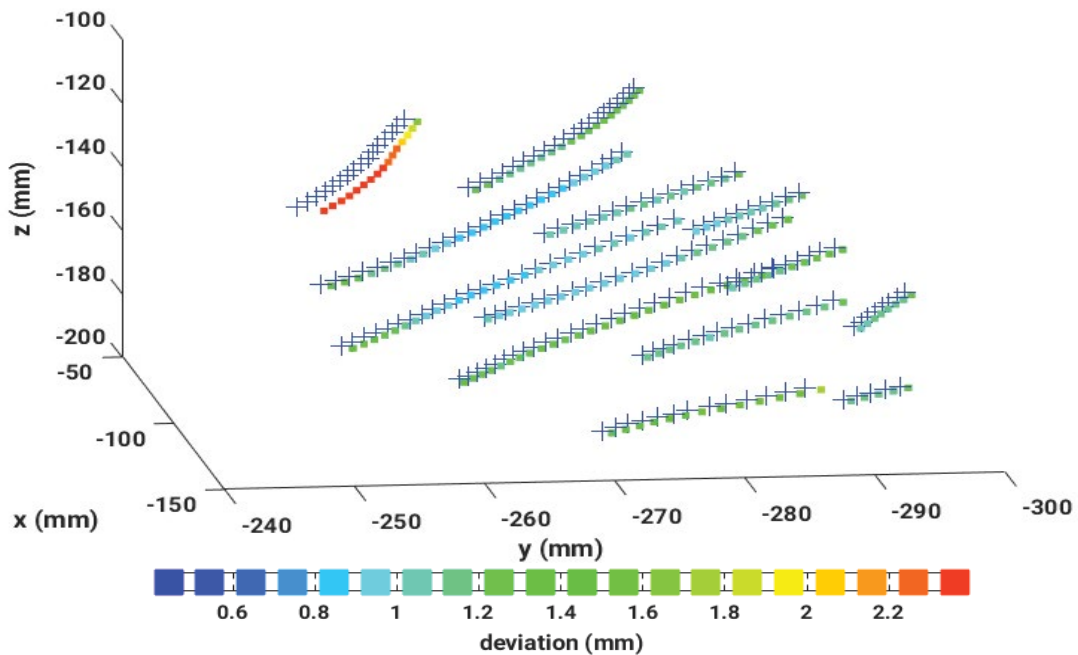


Figure 13: Dwell positions from both the CT and EMT data set. One catheter (red colored) clearly changed its position. Deviations are color-coded as shown

Alpha-stable distributions

Also histograms of dwell position deviations are generally right skewed, thus being reminiscent of α -stable distributions (a class of Levy distributions) [59-62]. In the frequency domain, this family of distributions is identified through its characteristic function $\varphi(\omega)$ given by:

$$\Phi(\omega) = \Phi_0^{(\alpha)}(\omega) \exp(i \mu \omega) \tag{12}$$

Where,

$$\Phi_0^{(\alpha)}(\omega) = \begin{cases} \exp(-|\gamma\omega|^\alpha [1 - i \cdot \text{sign}(\omega) \cdot \beta \cdot \tan(\alpha \frac{\pi}{2})]), \text{ for } \alpha \neq 1 \\ \exp(-|\gamma\omega| [1 + i \cdot \text{sign}(\omega) \cdot \frac{2}{\pi} \beta \cdot \log(|\omega|)]), \text{ for } \alpha = 1 \end{cases} \quad (13)$$

The parameter $\alpha \in (0, 2)$ measures the *impulsiveness* and provides a measure of tail thickness, while the *skewness* $\beta \in [-1, +1]$ measures the degree and sign of asymmetry. Furthermore, $\gamma > 0$ denotes the *scale* parameter for dispersion and the allocation parameter is set by μ . Roughly $100 \ll 50000$ entries of the histograms are sufficient to obtain a stable parameterization of the distributions. The related α -stable distribution function is obtained via an inverse Fourier transform:

$$f_{\alpha,\beta}(X | \gamma, \mu) = F_\omega^{-1}[\Phi(\omega)](X) = \frac{1}{2} \int_{-\infty}^{\infty} e^{-i\omega y} \Phi(\omega) d\omega \quad (14)$$

The histograms discussed above can be represented as a mixture of J α -stable probability density functions $f_{\alpha,\beta}(x|\gamma,\mu)$ according to Salas-Gonzalez et al. [63]:

$$p_X(X) = \sum_{j=1}^J \omega_j f_{\alpha_j,\beta_j}(X | \gamma_j, \mu_j), 0 \leq \omega_j \leq 1 \forall j \text{ and } \sum_{j=1}^J \omega_j = 1 \quad (15)$$

Where, $p_X(x)$ denotes the probability density function (pdf) of the vector x of dwell position deviations. Each component j carries a mixture weight ω_j and is related to an allocation variable $z_j \in [1, 2, \dots, k]$ via [64].

$$P(Z_j=j) = \omega_j \text{ for } j=1, \dots, J \quad (16)$$

Employing the Bayes' rule,

$$p(\theta | x) = \frac{p(x | \theta) p(\theta)}{p(x)} \propto p(x | \theta) p(\theta) \quad (17)$$

$$\theta = \{ \omega_{zi}, \gamma_{zi}, \mu_{zi}, \alpha_{zi}, J \},$$

The available data x and the prior information $p(\theta)$ are used to estimate the posterior probability $p(\theta|x)$ of the unknown quantities θ in a hierarchical model. The unknown parameters are estimated, at every iteration, using the Markov Chain Monte Carlo (MCMC) scheme with Gibbs sampling [63]. An example of the statistical analysis of the estimated dwell position deviations is demonstrated in Figure 15. The distribution is unimodal but asymmetric and is well approximated by α -stable distribution. However, the same data set also contained four histograms, related with the y -components of the dwell position deviations, which were identified as bi-modally distributed by a Hartigan Dip test. Consequently, the histogram was fit with a bi-modal α -stable distribution (Figure 15).

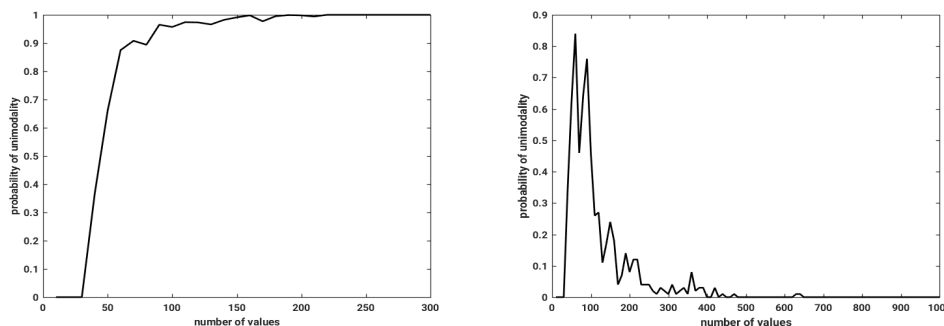


Figure 14: Shown are p-values for Left: an uni-modal distribution and Right: a bi-modal distribution of deviations of EMT-wise measured dwell positions from the CT reference data set

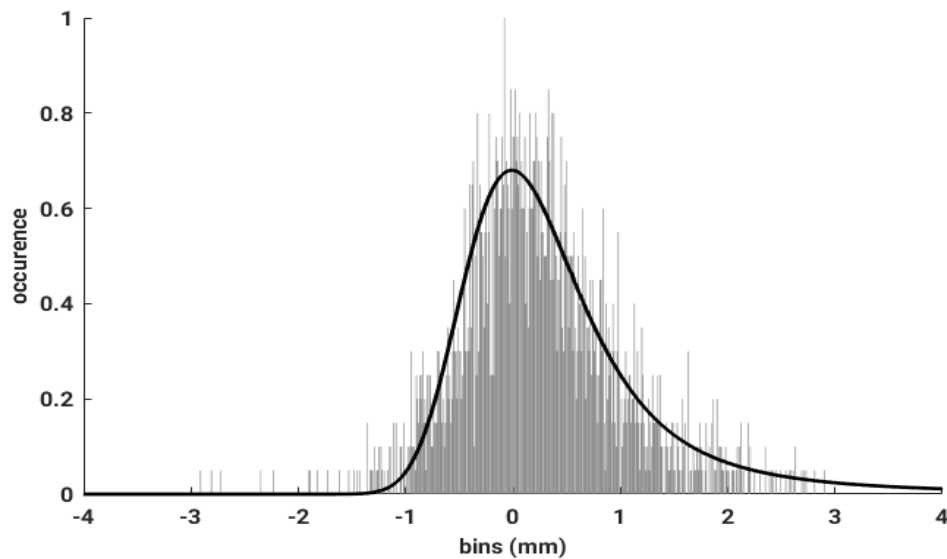


Figure 15: Histogram of the calculated deviations from the first dwell position in x-direction and its fit to an unimodal α -stable distribution

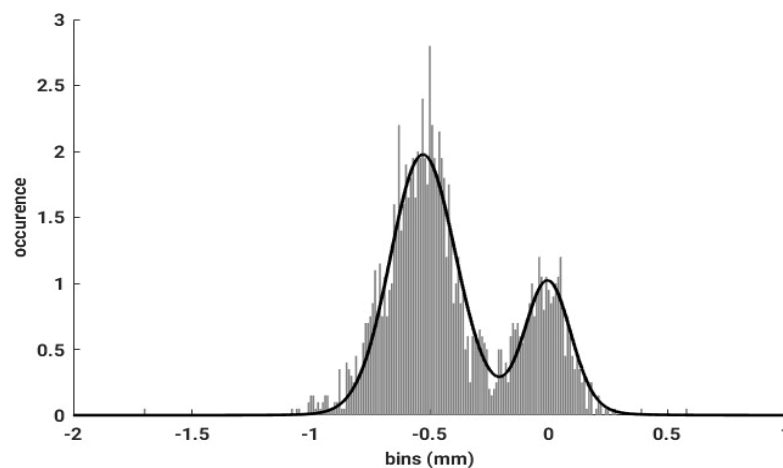


Figure 16: Histogram of the calculated deviations from the 111-th dwell position in y-direction and its fit to a bi-modal α -stable distribution

SUMMARY

We presented an expert system for the analysis of EMT data collected during a HDR-BT based on our most recent studies of this subject. The signal processing chain of this expert system is based on information-theoretic concepts and machine learning techniques and encompasses:

- Particle filter tracking of the state space trajectory of solenoid sensors inside catheters provide exact dwell positions without any noise contaminations.
- Singular spectrum analysis (SSA) for noise reduction and high amplitude technical artifact removal. Noise suppression is especially important in case of EMT fiducial sensor signals collected as a reference of breathing mode contributions to the EMT sensor signals. But EMT sensor signals occasionally contain artifacts due to malfunctioning of the EMT measurement device, which also can be easily removed with SSA.
- Ensemble empirical mode decomposition (EEMD) is employed to decompose both the fiducial and solenoid sensor signals into intrinsic oscillatory components.
- Similarity measures based on point-wise correlations or on entropy-based divergences between distributions identify breathing mode contributions in the solenoid sensor signals, which can be removed by neglecting them during signal reconstruction.

- Multi-dimensional scaling (MDS) to render dwell positions of solenoid sensors inside implanted catheters recorded during control measurements comparable to corresponding dwell positions established via an X-ray CT imaging in a treatment plan.

We demonstrated with illustrative examples the potential of the proposed signal processing chain in dealing with all signal analysis aspects encountered during an HDR-BT treatment.

ACKNOWLEDGEMENT

The presented work was performed in partial fulfillment of the requirements for obtaining the degree Dr. rer. nat. at the Friedrich-Alexander-Universität (FAU) Erlangen Nürnberg.

REFERENCES

1. Zhou J, Zamdborg L, Sebastian E. Review of advanced catheter technologies in radiation oncology brachytherapy procedures. *Cancer Manag Res*, **2015**, 7: 199-211.
2. Njeh F, Saunders MW, Langton CM. Accelerated partial breast irradiation (APBI): A review of available techniques. *Radiat Oncol*, **2010**, 5: 90.
3. Shah C, Wobb J, Manyam B, Khan A, Vicini F. Accelerated partial breast irradiation utilizing brachytherapy: Patient selection and workflow. *J Contemp Brachyther*, **2016**, 8: 90-94.
4. Okamoto H, Aikawa A, Yoshio K, Murakami N, Nakamura S, et al. Dose error from deviation of dwell time and source position for high dose rate Ir-192 in remote after loading system. *J Radiat Res*, **2014**, 55: 780-787.
5. Poulin N, Varfalvy S, Aubin, Beaulieu L. Comparison of dose and catheter optimization algorithms in prostate high-dose-rate brachytherapy. *Brachytherapy*, **2016**, 15:102-111.
6. Götz TI, Ermer M, Salas-González D, Kellermeier M, Strnad V, et al. On the use of multi-dimensional scaling and electromagnetic tracking in high dose rate brachytherapy. *Phys Med Biol*, **2017**.
7. Götz TI, Lahmer G, Brandt T, Kallis K, Strnad V, et al. electromagnetic tracking in high dose rate brachytherapy. *Phys Med Biol*, **2017b**, 62: 7617-7640.
8. Götz TI, Lahmer G, Strnad V, Bert C, Hensel B, et al. A tool to automatically analyze electromagnetic tracking data from high dose rate brachytherapy of breast cancer patients. *PLoS One*, **2017**, 12: 1-31.
9. Myronenko A, Song X. Point set registration: Coherent point drift. *IEEE Trans Pattern Anal Mach Intell*, **2010**, 32: 2262-2275.
10. Kellermeier M, Hofmann B, Strnad V, Bert C. Assessment of the implant geometry in fractionated interstitial HDR breast brachytherapy. *Brachytherapy*, **2016**, 15:S39-S40.
11. Kellermeier M, Herbolzheimer J, Kreppner S, Lotter M, Strnad V, et al. Electromagnetic tracking (EMT) technology for improved treatment quality assurance in interstitial brachytherapy. *J Appl Clin Med Phys*, **2017**, 18: 211-222.
12. Bert C, Kellermeier M, Tanderup K. Electromagnetic tracking for treatment verification in interstitial brachytherapy. *J Contemp Brachyther*, **2016**, 8: 448-453.
13. Harish V, Baksh A, Ungi T, Lasso A, Baum Z, et al. Measurement of electromagnetic tracking error in a navigated breast surgery setup. In SPIE Proceedings 9786, Medical Imaging, page 97862K, San Diego, Ca, USA, SPIE Digital Library. **2016**.
14. Liu L, Prasad SC, Bassano DA, Heavern J, Keshler B, et al. A dwell position verification method for high dose rate brachytherapy. *J Appl Clin Med Phys*, **2004**, 5: 1-5.
15. Jursinic PA. Quality assurance measurements for high-dose-rate brachytherapy without film. *J Appl Clin Med Phys*, **2014**, 15: 246-258.
16. Haidegger FT, Birkfellner W, Cleary K, Peters T, Maier-Hein L. Electromagnetic tracking in medicine: A review of technology, validation and applications. *IEEE Trans Med Imaging*, **2014**, 33: 1702-1725.
17. Bharat S, Kung C, Dehghan E, Ravi A, Venugopal N, et al. Electromagnetic tracking for catheter reconstruction in ultrasound-guided high-dose-rate brachytherapy of the prostate. *Brachytherapy*, **2014**, 13: 640-650.

18. Poulin E, Varfalvy N, Aubin S, Beaulieu L. Comparison of dose and catheter optimization algorithms in prostate high-dose-rate brachytherapy. *Brachytherapy*, **2015**, 15: 102-111.
19. Damato L, Viswanathan AN, Don SM, Hansen JL, Cormack RA. A system to use electromagnetic tracking for the quality assurance of brachytherapy catheter digitization. *Med Phys*, **2014**, 41: 101702.
20. Balachandran R, Fitzpatrick JM. Iterative solution for rigid-body point-based registration with anisotropic weighting. In Proceedings of SPIE, Medical Imaging, Visualization, Image-Guided Procedures and Modeling, M. I. Miga, K. H. Wong (edtrs.), *SPIE*, **2009**.
21. Danilchenko A, Wiles AD, Balachandran R, Fitzpatrick JM. Improved method for point-based tracking. *Med Image Comput Comput Assist Interv*, **2010**, 13: 587-594.
22. Kindratenko V. A survey of electromagnetic position tracker calibration techniques. *Virtual Real*, **2000**, 5: 169-182.
23. Sadjadi H, Hashtrudi-Zaad K, Fichtinger G. Simultaneous electromagnetic tracking and calibration for dynamic field distortion compensation. *IEEE Trans Biomed Eng*, **2016** 63: 1771-1781.
24. Beeksmas B. Source tracking and quality assurance of high dose rate (HDR) brachytherapy. In: Master of Science, Research thesis, Centre for Medical Radiation Physics. University of Wollongong, **2014**.
25. Cox MAA, Cox TF. Multidimensional scaling. Chapman and Hall, **1994**.
26. Borg I, Groenen PJF. Modern multidimensional scaling. Springer Series in Statistics, **2005**.
27. Abdi H. Metric multidimensional scaling (MDS): Analyzing distance matrices. In: Encyclopedia of Measurement and Statistics, Nell Salkind, Sage, CA, USA, **2007**.
28. Arulampalam MS, Maskell S, Gordon N, Clapp T. A tutorial on particle filters for online non-linear, non-Gaussian Bayesian tracking. *IEEE Trans Signal Process*, **2002**, 50: 174-188.
29. Gustafsson F. Particle filters theory and practice with positioning applications. *IEEE Aerospace and Electronic Systems Magazine*, **2010**, 25: 53-82.
30. Golyandina N, Nekrutkin V, Zhigljavsky A. Analysis of time series structure: SSA and related techniques. Chapman and Hall, CRC, **2001**.
31. Ghil M, Allen MR, Dettinger MD, Ide K, Kondrashov D, et al. Advanced spectral methods for climatic time series. *Rev Geophys*, **2002**, 40.
32. Teixeira AR, Tomé AM, Göhm M, Puntonet CG, Lang EW. How to apply non-linear subspace techniques to univariate biomedical time series. *IEEE Trans Instrument Measur*, **2009**, 58: 2433-2443.
33. Tomé M, Teixeira AR, Figueiredo N, Santo IM, Georgieva P, Lang EW. SSA of biomedical signals: A linear invariant systems approach. *Statistics and Its Interface*, **2010**, 3: 345-355.
34. Huang NE, Shen Z, Long SR, Wu MC, Shih HH, et al. The empirical mode decomposition and the Hilbert spectrum for non-linear and non-stationary time series analysis. In: Proceedings of Royal Society of London A: Mathematical, Physical and Engineering Sciences, **1998**, 454.
35. Wu Z, Huang NE. Ensemble empirical mode decomposition: A noise-assisted data analysis method. *Adv Adapt Data Anal*, **2009**, 01:1-41.
36. Zeiler A, Faltermeier R, Tomé AM, Keck IR, Puntonet C, et al. Sliding empirical mode decomposition-brain status data analysis and modeling. In: Advances in Intelligent Signal Processing and Data Mining, Georgieva P, Mihaylova L, Jain LC (eds.), Springer-Verlag Berlin Heidelberg, **2012**.
37. Rehman N, Park C, Huang NE, Mandic DP. EEMD via NA-MEMD: Multivariate noise-aided computation of standard EMD. *Adv Adapt Data Anal*, **2013**, 5: 1-25.
38. Liu JS, Chen R. Sequential Monte Carlo methods for dynamic systems. *J Am Stat Assoc*, **1998**, 93.
39. Andrieu C, Doucet A, Holenstein R. Particle Markov chain Monte Carlo methods. *J R Stat Soc B*, **2010**, 72: 269-342.
40. Doucet A, Johansen AM. A tutorial on particle filtering and smoothing: Fifteen years later. **2012**.
41. Todkar S, Kass RE. Importance sampling: A review. *Adv Rev*, **2008**.

-
42. Gordon N, Salmond D, Smith A. Novel approach to nonlinear, non-Gaussian Bayesian state estimation. *Radar Signal Process IEE Proc*, **1993**, 140: 107-113.
 43. Teixeira R, Tomé AM, Lang EW. Unsupervised feature extraction via kernel subspace techniques. *Neurocomputing*, **2011**, 74: 820-830.
 44. Hassani H. Singular spectrum analysis: Methodology and comparison. *J Data Sci*, **2007**, 5: 239-257.
 45. Hemakom LA, Mandic DP. Intrinsic multi-scale analysis: A multivariate EMD framework. *Proc R Soc A*, **2014**, 471: 1-28.
 46. Al-Subari K, Al-Baddai S, Tomé A, Volberg G, Hammwöhner R, et al. Ensemble empirical mode decomposition analysis of EEG data collected during a contour integration task. *PLoS One*, **2015**, 10: e0119489.
 47. Faltermeier R, Zeiler A, Tomé AM, Brawanski A, Lang EW. Weighted sliding empirical mode decomposition. *Adv Adapt Data Anal*, **2011**, 3: 509-526.
 48. Pearson K. Notes on regression and inheritance in the case of two parents. *Proc R Soc Lond*, **1895**, 58: 240-242.
 49. Shannon CE. The mathematical theory of communication. In *The Mathematical Theory of Communication*, C.E. Shannon, W. Weaver (eds.) University of Illinois Press, **1998**.
 50. Gel'fand M, Yaglom AM. Calculation of the amount of information about a random function contained in another such function. *Am Math Soc Trans*, **1959**, 2: 199-246.
 51. Taneja J. New developments in generalized information measures. *Adv Imaging Electron Phys*, **1995**, 91: 37-135.
 52. Kullback S, Leibler RA. On information and sufficiency. *Ann Math Stat*, **1951**, 22: 79-86.
 53. Lin J. Divergence measures based on the Shannon entropy. *IEEE Tran Inform Theory*, **1991**, 37: 145-151.
 54. Deza E, Deza MM. *Dictionary of distances*. Elsevier, **2006**.
 55. Williams KJ. On a connection between kernel Pca and metric multidimensional scaling. *Machine Learn*, **2002**, 46: 11-19.
 56. Golub GH, van Loan CF. *Matrix computations*. John Hopkins University Press, **1989**.
 57. Hartigan J, Hartigan P. The dip test of unimodality. *Ann Statist*, **1985**, 13: 70-84.
 58. Hartigan P. Algorithm AS 217: Computation of the dip statistic to test for unimodality. *J R Stat Soc Series C*, **1985**, 34: 320-325.
 59. Nolan J. *Stable distributions: Models for heavy-tailed data*. Springer, New York, **2016**.
 60. Coles S. *An introduction to statistical modeling of extreme values*. Springer Verlag, Berlin, **2001**.
 61. Sato KI. *Lévy processes and infinite divisibility*. Cambridge University Press, Cambridge, **1999**.
 62. Salas-Gonzalez D, Kuruoglu EE, Ruiz DP. Finite mixture of α -stable distributions. *Digital Signal Process*, **2009**, 19: 250-264.
 63. Salas-Gonzalez D, Kuruoglu EE, Ruiz DP. Modeling with mixture of symmetric stable distributions using Gibbs sampling. *Signal Process*, **2010**, 90: 774-783.
 64. Salas-Gonzalez D, Schlögl M, Górriz JM, Ramírez J, Lang EW. Bayesian segmentation of magnetic resonance images using the α -stable distribution. In: *International Conference on Hybrid Artificial Intelligence Systems*, Springer, **2011**.